Fullerenol-Based Electroactive Artificial Muscles Utilizing Biocompatible Polyetherimide

Mahendran Rajagopalan and Il-Kwon Oh*

Division of Ocean Systems Engineering, School of Mechanical, Aerospace and Systems Engineering, Korea Advanced Institute of Science and Technology, 291 Daehak-ro, Yuseong-gu, Daejeon 305-701, Republic of Korea

ABSTRACT Two essential functional requirements for electroactive artificial muscles, which can be used for biomedical active devices, are biocompatibility and sufficient range of motion. Fullerenol nanoparticles and their derivatives have been validated as potential candidates to be used for nanobiomaterials and biomedical applications because of their excellent proton conductivity, hydrophilicity, and biocompatibility. We developed fullerenol-based electroactive artificial muscles utilizing biocompatible polyetherimide. By using a solvent recasting method, present ionic networking membranes have been successfully synthesized with homogeneous dispersion of polyhydroxylated fullerene (PHF) nanoparticles into a sulfonated polyetherimide (SPEI) matrix. In comparison with pure SPEI membranes, the PHF–SPEI nanocomposite membranes show much higher water uptake and proton conductivity, which are both essential characteristics for high-performance ionic polymer actuators. The developed PHF–SPEI actuator shows over three times larger motion ranges and two times higher blocking forces than the pure SPEI actuator. The excellent biocompatibility of PHF and SPEI makes these actuators promising candidate materials for biomedical devices such as active stents and catheters.

KEYWORDS: fullerenol · polyetherimide · actuators · biocompatibility · proton conductivity

A fullerene nanomaterial is a nanoscale sphere or ellipsoid molecule composed entirely of carbon atoms. Spherical fullerenes are also called buckyballs, and cylindrical carbon structures are called carbon nanotubes or buckytubes and they exhibit a pentagonal or heptagonal carbon ring structure similar to graphite, which is composed of stacked graphene sheets of linked hexagonal rings. The first fullerene to be discovered was buckminster fullerene (C_{60}), which was prepared in 1985 by Richard Smalley, Robert Curl, and Harold Kroto,[1] who were awarded the 1996 Nobel Prize in chemistry. Since their discovery, fullerenes have been a hot topic in the field of nanoscience and nanotechnology because of their outstanding chemical and physical properties. Fullerenes have been investigated for potential use as medicine,[2] as light-activated antimicrobial agents,[3] for heat resistance,[4] for superconductivity,[5] as proton conductors,[6] and for biocompatibility.[7]

Fullerene nanomaterials have been applied to photovoltaic devices,[8] biomedical devices,[9] fuel cells,[10−12] gas separation membranes,[13,14] and more. It has been shown that incorporating fullerenes into a polymer matrix improves proton conductivity and thermomechanical stability and suppresses thermo-oxidative degradation of the host polymer.[15−18] Fullerenes are usually produced in a powdery form that protects their practical applications in fuel cells, photovoltaic cells, and so on. In order to overcome this drawback, fullerenes are reinforced into the polymer matrix to obtain a smart material for practical applications. The literature has identified several techniques for linking fullerenes with polymers,[18,19] with physical blending being one of the simplest techniques.[20] However, the poor adhesion and low miscibility of fullerene (C_{60}) in common organic solvents typically prevent it from being well-dispersed in a polymer matrix. In order to overcome these difficulties, the fullerenes are functionalized with hydrophilic groups, which enhance their physicochemical properties while promoting thorough dispersion and strong adherence in the polymer matrix.

Fullerenol (polyhydroxylated fullerene, PHF) offers superior hydrophilic nature, high proton conductivity, excellent medicinal properties,[21−23] improved miscibility in host polymers without significant agglomeration, and enhanced water uptake property in host polymers, all of which are essential characteristics for electroactive ionic polymer actuators. It has been reported that fullerene–nafion composite membranes showed higher proton conductivity and improved water uptake property compared to the pristine nafion membrane.[20]

* Address correspondence to ikoh@kaist.ac.kr.

Received for review December 18, 2010 and accepted February 10, 2011.

Published online February 18, 2011
10.1021/nn103521g

TABLE 1. Physicochemical Properties of SPEI, PHF−SPEI, and Fullerene−SPEI Membranes

membrane code	SPEI (wt %)	PHF (wt %)	water uptake (g/g)	IEC (mequiv/g)	proton conductivity (S/cm)	blocked force (g_f)	thickness (μm)
SPEI	10		0.264	0.553	0.0014	0.355	198[28]
PHF−SPEI **1**	10	0.1	0.314	0.498	0.0024	0.375	184
PHF−SPEI **2**	10	0.3	0.346	0.522	0.0041	0.559	189
PHF−SPEI **3**	10	0.5	0.365	0.562	0.0127	0.673	179
fullerene−SPEI	10	0.5	0.258	0.512	0.0110	0.604	181

Chiang *et al.* synthesized fullerenol cross-linked polyurethane starburst polymers, which possessed superior thermomechanical stability compared to pure polyurethane.[24] Recently, Ouyang *et al.* prepared fullerenol/amino-terminated polydimethyl siloxane supramolecular assembled nanocomposites which exhibited strong hydrogen-bonding interactions between the reactants and excellent mechanical stability.[25] The fullerenols are also biocompatible, and they feature many medicinal properties. All of these outstanding traits make these materials ideal for biomedical devices and applications.[26,27]

Recently, sulfonated polyetherimide (SPEI) has been proven as a novel electroactive polymer for electromechanical actuators[28] because of its excellent mechanothermal stability, cost effectiveness, reliable film-forming properties, reasonable water uptake and ionic exchange capacity, and superior biocompatibility.[28−34] In addition, the sulfonic acid group makes it possible to execute hydrogen bonding with functionalized hydrophilic nanoparticles.[35] The performance of nanocomposite ionic polymer actuators depends largely on their proton conductivity, migration of water molecules, mobility of cations through nanochannels inside the ionic polymer membrane, and physicochemical properties of the materials.

In this study, we have developed biocompatible electroactive artificial muscles based on fullerenol and sulfonated polyetherimide. The combination of PHF and SPEI offers critical advantages in terms of biocompatibility, hydrophilicity, physical bonding, and high proton conductivity, resulting in high-performance artificial muscle actuators. To the best of our knowledge, fullerenol has not yet been used for electro-ctive polymer actuators. The PHF−SPEI composite membranes were fabricated by using a solution recasting method for homogeneous dispersion of fullerenol nanoparticles in the polymer matrix.

The dispersion and the agglomeration of PHF particles in the SPEI matrix were observed using image tools such as a field emission scanning electron microscopy (FE-SEM) and atomic force microscopy (AFM). The incorporation of the PHF enhanced both the physicochemical properties and the biocompatibility of the SPEI, indicating that these nanocomposite membranes would be a potential candidate for future biomedical active devices.

RESULTS AND DISCUSSION

Table 1 shows the weight ratio of PHF/fullerene in the SPEI solution, as well as the thickness and physicochemical properties of PHF−SPEI **1** (0.1 wt %), PHF−SPEI **2** (0.3 wt %), PHF−SPEI **3** (0.5 wt %) (for convenience, these membrane compositions are denoted as PHF-SPEI **1**−**3**, respectively), and fullerene−SPEI (0.5 wt %) membranes. The water uptake ratio, which is an essential parameter for the bending motions of wet electromechanical actuators, increased as the weight ratio of PHF in the polymer matrix increased, owing to the excellent hydrophilic nature of PHFs.[36,37] The enhancement of the water uptake ratio from PHF−SPEI **1** (0.314 g/g) to PHF−SPEI **3** (0.365 g/g) influences the large bending deformation of the PHF−SPEI **1**−**3** actuators because of the movement of water molecules under the electric field inside the actuators. On the contrary, the water uptake ratio of the fullerene−SPEI membrane did not change significantly, perhaps due to the hydrophobic nature of fullerenes. Because the PHFs and fullerenes are weakly acidic in nature, the ionic exchange capacity (IEC) of the PHF−SPEI **1**−**3** and fullerene−SPEI membranes did not vary. In contrast, the proton conductivity of the PHF−SPEI and fullerene−SPEI composite membranes drastically increased along with the increasing weight ratio of PHF in the polymer solution. The observed proton conductivities were 0.0024, 0.0041, 0.0127, and 0.0110 S/cm for PHF−SPEI **1**−**3** and fullerene−SPEI membranes, respectively. It can be concluded that the PHFs and fullerenes are excellent proton conductors[15,16] since increasing their weight ratio in the polymer solution led to enhanced proton conductivity in the SPEI composite membranes.

Figure 1 shows images of the pristine PHF−SPEI **1**−3 (a, b, and c) membranes, which changed in color from yellowish to black with respect to the loading level of PHF in the SPEI matrix. This might be due to the visible region absorption of C═C bonds in the PHF, owing to the average number of C═C double bonds being increased by increasing the weight ratio of PHF, which consequently enhanced $\pi-\pi$ conjugation in the fullerene cage.[37]

The FT-IR spectra of SPEI, PHF, and PHF−SPEI are shown in Figure 2. In the PHF spectra, the hydroxyl group appeared as a broad absorption band around 3400 cm^{-1}, C═C bands appeared at 1600 cm^{-1}, O−H

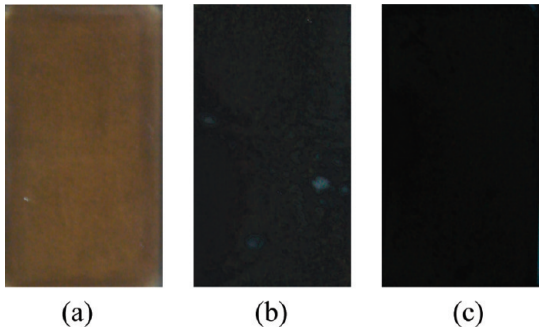

Figure 1. Photographs of PHF−SPEI 1−3 (a−c) membranes.

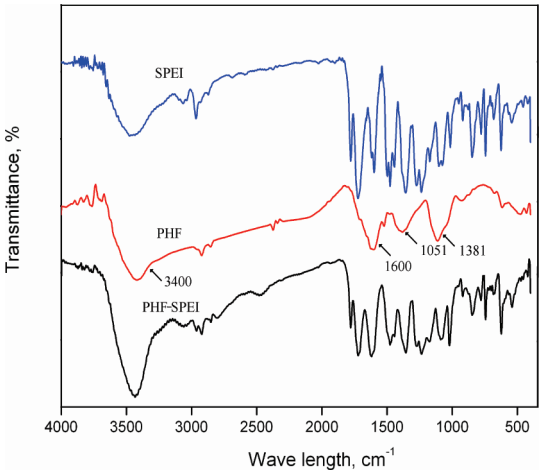

Figure 2. FT-IR spectra of SPEI, PHF, and PHF−SPEI composite.

bending vibration appeared at 1381 cm^{-1}, and a C−O stretching band appeared at 1112 cm^{-1}.[38,39] In the PHF−SPEI spectra, the broadening band absorption of the hydroxyl group from 3300 to 3700 cm^{-1} confirmed the incorporation of PHF in the SPEI matrix, demonstrating the formation of weak intermolecular hydrogen bonding between the sulfonic acid group of SPEI and the hydroxyl group of PHF. The intense peak of the O−H bending vibration around 1355 cm^{-1} further confirmed the interaction between these two groups in the PHF−SPEI membranes.[40]

Figure 3 represents the thermogravimetric analysis of the SPEI, PHF, and PHF−SPEI composite. The weight loss of the SPEI occurred in three stages: initial weight loss started at 100 °C due to the loss of water molecules; another weight loss occurred at 280 °C because of the loss of sulfonic acid groups from the polymer backbone; and the final weight loss around 530 °C was possibly due to the decomposition temperature of the PEI chain.[28] In the PHF, the weight loss around 100 °C was again caused by the elimination of water, while the weight loss around 200 °C was most likely due to the degradation temperature of PHF. In the PHF−SPEI composite, the weight loss occurred in four stages: at 100 °C, due to the elimination of water molecules; at 200 °C, due to the decomposition temperature of PHF

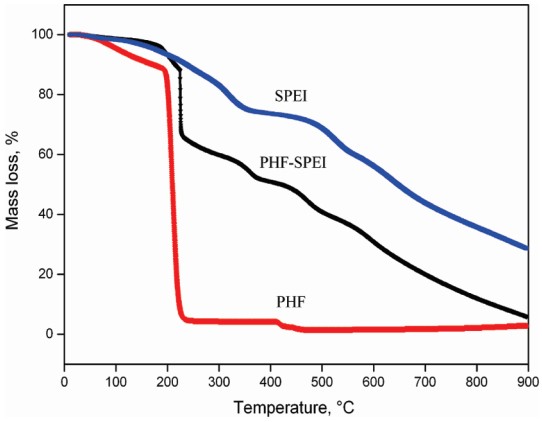

Figure 3. TGA of SPEI, PHF, and PHF−SPEI composite.

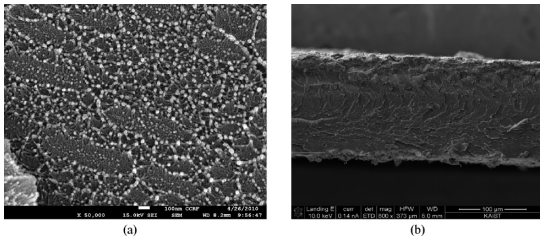

Figure 4. SEM micrographs: cross-sectional images of fullerene−SPEI (0.1 wt %) membrane (a); platinum-coated fullerene−SPEI (0.1 wt %) membrane (b).

molecules by nearly 400 °C; around 380 °C, due to the elimination of the sulfonic acid group from the SPEI backbone; and at 530 °C, due to the decomposition temperature of the PEI chain. Hence, the incorporation of the PHF into the SPEI matrix was clearly confirmed by both thermogravimetric analysis and the FT-IR spectra.[25,39]

Figure 4 shows the SEM images of fullerene (0.1 wt %)−SPEI (a) and platinum-coated fullerene−SPEI (b) membranes. The agglomeration of fullerenes was higher than that of PHFs in the SPEI matrix, which indicates that the hydrophobic nature of the fullerenes suppressed their dispersion in the hydrophilic SPEI matrix. The thickness of the platinum layer on the surface of the membrane was observed to be around 10−15 μm. Figure 5a−d shows the cross-sectional morphology of pristine PHF−SPEI **1** and Pt-coated PHF−SPEI **1** membranes. In the PHF−SPEI **1** membrane, the PHFs were homogeneously dispersed in the SPEI matrix, as shown in Figure 5b,c. This likely occurred because of the hydrophilic−hydrophilic interaction between the sulfonic acid group of the SPEI and the hydroxyl group in PHF, which improved the miscibility and reduced the agglomeration of the PHF in the polymer matrix.[41] The average particle size of the PHF in the polymer matrix was 15−30 nm, and most of the particles were in spherical shape. The thickness of the Pt layer on the membrane surface was around 12−17 μm.

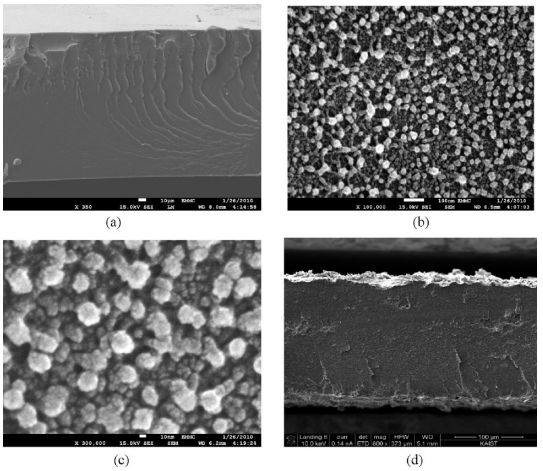

Figure 5. SEM micrographs: cross-sectional images of PHF−SPEI 1 (a−c) and platinum-coated PHF−SPEI 1 membrane (d).

Tapping mode AFM images of the fullerene−SPEI membrane are shown in Figure 6. The agglomeration of fullerene in the polymer matrix can be clearly observed from the large and irregular grains on the surface of the membrane. Figure 7a−f shows the top view and 3D mode images of the PHF−SPEI **1**−**3** membranes, and the images of the composite membrane indicate that the agglomeration of PHF in the SPEI matrix increased along with the increasing weight ratio of PHF in the SPEI matrix, as can be seen by the small and regular grains.[42,43] These grains may have formed because of the aggregation of PHF molecules on the surface of the SPEI membranes, due to the weak intermolecular hydrogen bonding between the −OH group of PHF and the $-SO_3H$ group of SPEI. Compared with the fullerene−SPEI membrane, the agglomeration of PHFs in the SPEI matrix is negligible.

Figure 8 shows the harmonic responses of the SPEI and PHF−SPEI **1**−**3** actuators under an applied voltage of AC 4 V at an excitation frequency of 0.1 Hz (Figure 8a) and the PHF−SPEI **3** actuators at AC 1−4 V at the same excitation frequency (Figure 8b). The tip displacement of the PHF−SPEI **3** actuator, which had the highest weight ratio of PHF (0.5 wt %), was 1.82 mm, which was approximately three times more than the pristine SPEI actuator with tip displacement of 0.59 mm under the input voltage of 4 V. The tip displacements of the PHF−SPEI **1** and PHF−SPEI **2** actuators were observed at 1.06 and 1.4 mm, respectively. This finding indicates that the high proton conductivity and superior hydrophilic nature of PHF had a considerable influence on the bending motion of the PHF−SPEI actuators.[11,12] Notably, under hydrated conditions, the nanochannels in the SPEI polymer matrix enhance the diffusion of hydrated PHFs, protons, and water molecules under the electric field, resulting in the large bending deformation of the PHF−SPEI **1**−**3** actuators.[44−46] These nanochannels formed *via* the aggregation of

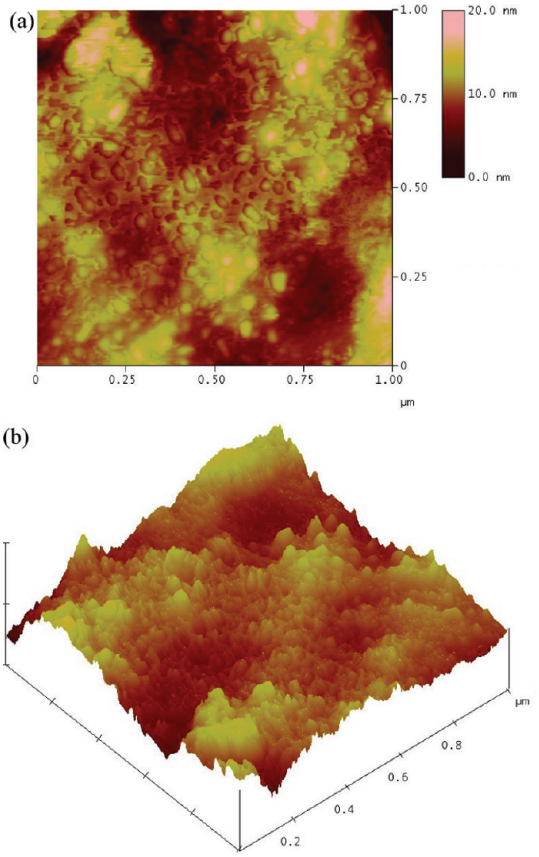

Figure 6. AFM images of fullerene−SPEI (a, top view; b, 3D phase mode) membrane.

hydrophilic groups/moieties in the ionic polymer chain.[46] In a recent study, Klaus and Chen proposed that the nanochannels in hydrated nafion membranes, which have a strong hydrophilic moiety in their polymeric backbones like sulfonic acid group, make a path for the diffusion of water molecules and proton inside the polymer matrix.[46] The relatively small quantity of PHF (0.5 wt %) in the polymer matrix still resulted in large bending deformations at the applied voltages from 1 to 4 V, which indicates that these nanocomposite actuators are promising candidates for future high-performance actuators. For comparison, the harmonic responses of SPEI, fullerene−SPEI, and PHF−SPEI **3** actuators are shown in Figure 9. Because of the excellent proton conductivity of PHFs and fullerene in the SPEI matrix, the PHF−SPEI **3** and fullerene−SPEI actuators showed larger tip displacement than the SPEI actuator.

Figure 10 shows the step response of the PHF−SPEI **3** actuator as recorded by an imaging solutions group camera connected to a Labview program. The DC excitation was carried out for SPEI and PHF−SPEI **1**−**3** actuators at 3 V at 0.1 Hz, as shown in Figure 11a. Figure 11b shows the step response of the PHF−SPEI **3** actuator from 2 to 4 V. As the excitation voltage was increased, the bending displacement of the actuators also increased with respect to the content of PHF in the

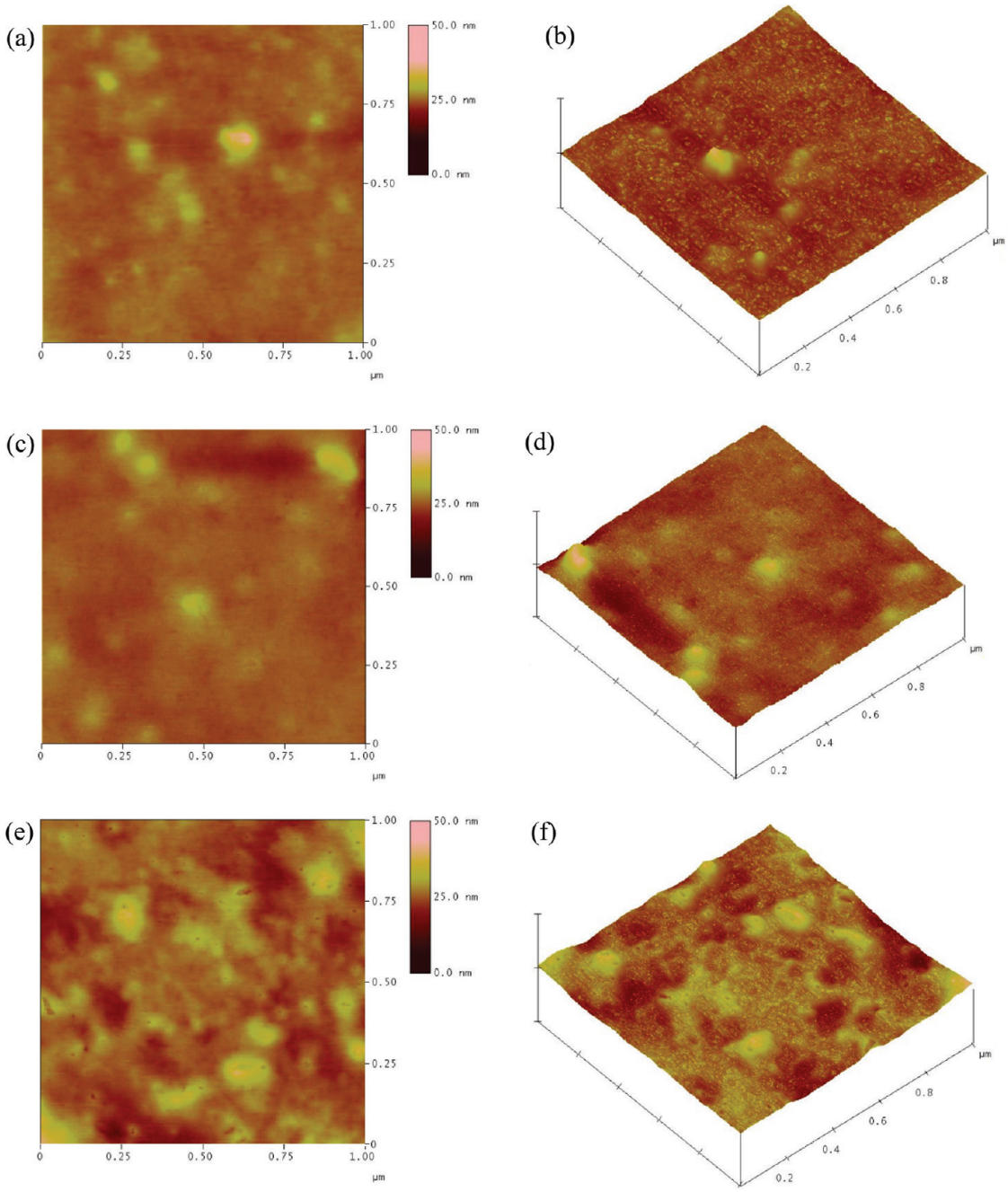

Figure 7. AFM images of PHF−SPEI 1 (a, top view; b, 3D phase mode), PHF−SPEI 2 (c, top view; d, 3D phase mode), and PHF−SPEI 3 (e, top view; f, 3D phase mode) membranes.

SPEI matrix. This increase can be attributed to the higher proton conductivity of PHF and the movement of the hydrated PHF in the nanochannels. By rapidly diffusing the hydrated PHFs, the nanochannels in the polymer matrix drastically influenced the bending deformation of the actuators under electric field. The PHF−SPEI **3** showed greater tip displacement than the other actuators under the electric field. Notably, the straightening-back phenomenon, which is one of the main drawbacks of conventional ionic polymer actuators, was not observed in any of the actuators because of the slow diffusion of the water molecules in the ionic nanochannel of nanocomposite networking membranes. The bending deformation of the PHF−SPEI **3** actuator increased as the applied voltage was increased from 2 to 4 V at 0.1 Hz, which could be due to the rapid movement of hydrated PHF through the ionic nanochannels in the ionic exchangeable membranes. The step responses of SPEI, fullerene−SPEI, and PHF−SPEI **3** at the excitation voltage of DC 5 V are shown in Figure 12. Because of the higher proton conductivity of PHF and fullerene, the PHF−SPEI **3** and fullerene−SPEI actuators showed greater bending deformation than the pristine SPEI actuator.

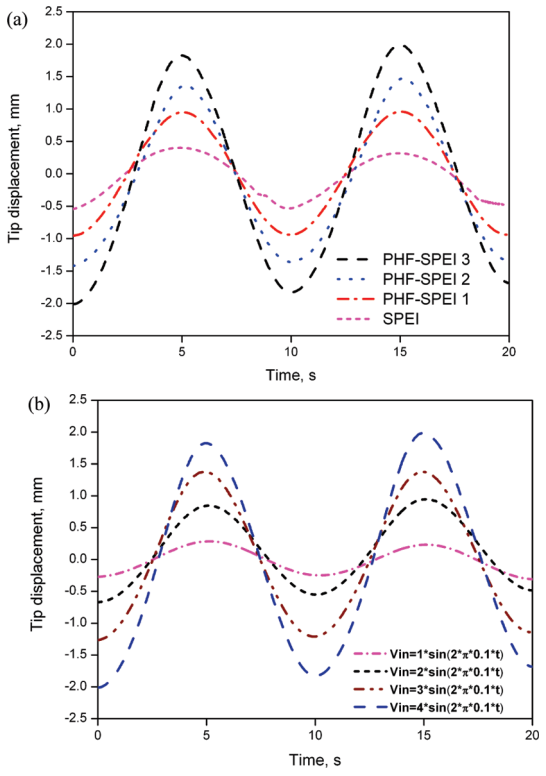

Figure 8. Harmonic responses of SPEI and PHF−SPEI actuators at 4 V (a); PHF−SPEI 3 actuator under sinusoidal inputs (b).

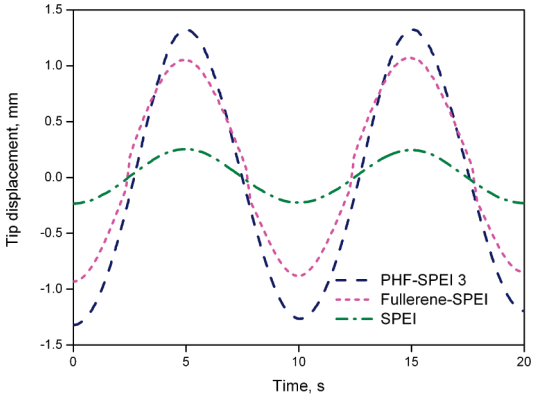

Figure 9. Harmonic responses of SPEI, fullerene−SPEI, and PHF−SPEI 3 actuators at 3 V.

The blocking forcec of the SPEI, fullerene−SPEI, and PHF−SPEI **1**−**3** actuators are listed in Table 1. The blocking force of PHF−SPEI **3** (0.673 g_f) was almost twice that of SPEI (0.355 g_f), and the PHF−SPEI **1** (0.375 g_f), PHF−SPEI **2** (0.559 g_f), and fullerene−SPEI (0.604 g_f) actuators also exhibited enhanced blocking forces compared to the pristine actuator. The increase in the weight ratio of PHF/fullerene in the polymer matrix likely enhanced the mechanical stiffness of these composite actuators, leading to a subsequent rise in the blocking force. Although these nanocomposite actuators possessed higher water content than the pristine actuator, the mechanical stability of the PHF/fullerene still influenced the movement of the actuators under electric field.

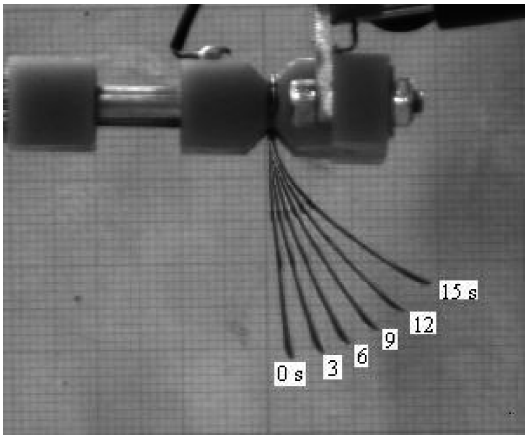

Figure 10. Actuation performance of PHF−SPEI 3 actuator under step response recorded by an imaging solutions group camera connected with the Labview program.

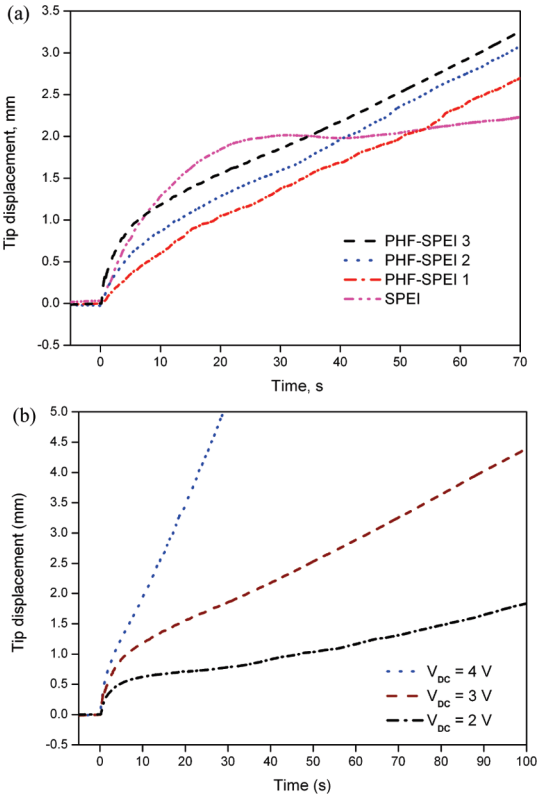

Figure 11. Step responses of SPEI and PHF−SPEI actuators at 3 V (a); PHF−SPEI 3 actuator under DC voltages (b).

Figure 13 shows current and voltage diagrams of the SPEI and PHF−SPEI **1**−**3** actuators at the applied voltage of 4 V at 0.1 Hz under sinusoidal wave input. The area of the circle corresponds to the dissipated electrical input energy of the actuator. The area of the circle increases with respect to the increasing content of PHF in the polymer matrix, and the PHF−SPEI **3** had

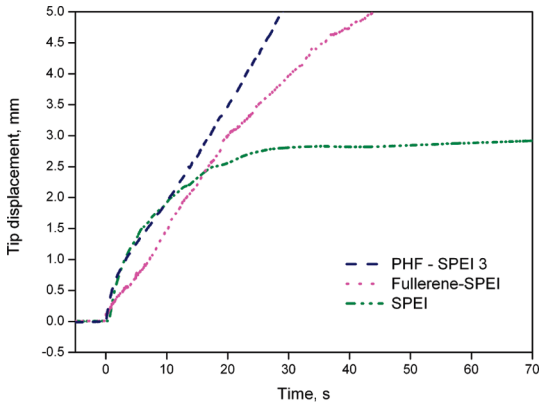

Figure 12. Step responses of SPEI, fullerene−SPEI, and PHF−SPEI 3 actuators at 5 V.

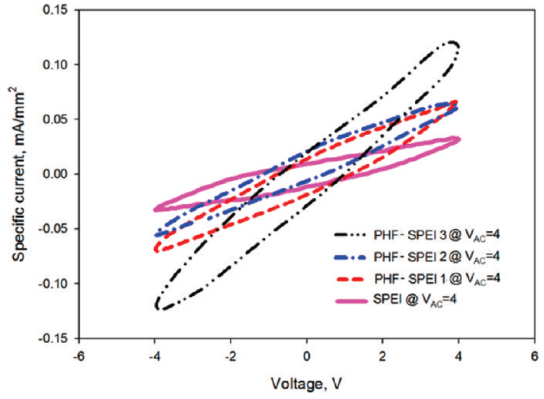

Figure 13. *V*−*I* diagram of SPEI and PHF−SPEI actuators.

the maximum value of the specific current at 0.125 mA/mm^2. Actuation durability of the SPEI and PHF−SPEI **1**−**3** actuators was assessed under sinusoidal excitation of 2 V at 0.1 Hz for 4 h, with the results shown in Figure 14. Due to the depletion of ions, as well as the deterioration of the platinum electrode over the extended operating time, the actuation performance of the actuators decreased with respect to time. Generally, PHF−SPEI actuators maintain much larger displacement in comparison with pure SPEI actuator.

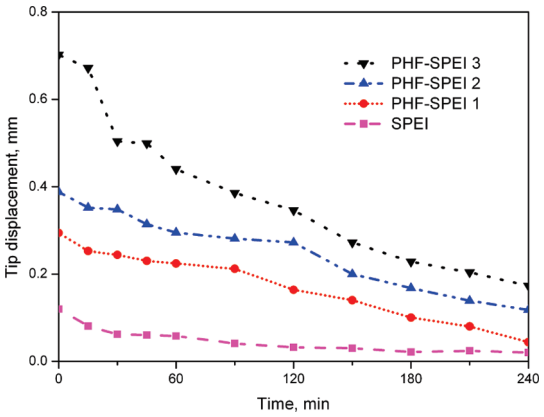

Figure 14. Durability of SPEI and PHF−SPEI actuators under sinusoidal input with a magnitude of 2 V and a frequency of 0.1 Hz.

CONCLUSION

We fabricated fullerenol-based electroactive artificial muscles utilizing biocompatible polyetherimide, resulting in large bending deformation and improved biocompatibility. The incorporation of minute quantities of PHF (0.5 wt %) into the SPEI matrix dramatically enhances the proton conductivity and water uptake property, both of which are vital parameters for high-performance ionic actuators. The dispersion of PHF particles in the SPEI matrix was superior to that of fullerene nanoparticles because of weak hydrogen bonding between the polar groups of PHF and SPEI. The PHF−SPEI actuators showed enhanced bending deformation under harmonic and step inputs as compared to the pristine SPEI actuator, and the PHF−SPEI actuators did not show the straightening-back phenomenon which is a critical drawback of ionic polymer actuators. The movement of hydrated PHFs in the nanoscale ionic channels of PHF−SPEI membranes results in much larger bending deformation under electric fields. Moreover, PHF and SPEI are biocompatible and eco-friendly, so these PHF−SPEI actuators are promising candidates for use in biomedical devices, artificial muscles, and biomimetic robots.

MATERIALS AND METHODS

PEI (Ultem 1000, Sigma-Aldrich, Republic of Korea) was dried in an oven at 130 °C overnight. Polyhydroxylated fullerene, dimethyl acetamide, buckminster fullerene (C_{60}), chlorosulfonic acid, and tetraamineplatinum chloride hydrate were purchased from Sigma-Aldrich, Republic of Korea, and used as-received. Sodium borohydride was obtained from Daejung Chemicals & Metals Co.

The sulfonation of polyetherimide can be found elsewhere.[28,29] The PHF−SPEI and fullerene−SPEI composite membranes were prepared by solution casting. Scheme 1 illustrates the preparation of the PHF−SPEI composite membranes. Briefly, the SPEI (10 wt %) was dissolved in DMAc and stirred rapidly at 40 °C for 4 h to obtain a homogeneous solution. Then, the PHF (at weight ratios of 0.1, 0.3, and 0.5 wt %) and fullerene (0.1 and 0.5 wt %) were added to the polymer solution and stirred overnight. The solution was poured into a Teflon mold and then kept in an oven at 80 °C overnight, and at 120 °C for 4 h, until the solvent was completely evaporated. The thickness of the as-prepared membranes was measured by a digital micrometer.

Structural analysis of the SPEI, PHF, and PHF−SPEI was characterized by Fourier transform infrared spectroscopy (FT-IR, SHIMADZU, IR Prestige-21), and their thermal stabilities were examined by thermogravimetric analysis under a nitrogen atmosphere (TGA/SDTA851e, Mettler Toledo). The hydrophilic nature of the PHF−SPEI **1**−**3** membranes was measured by a

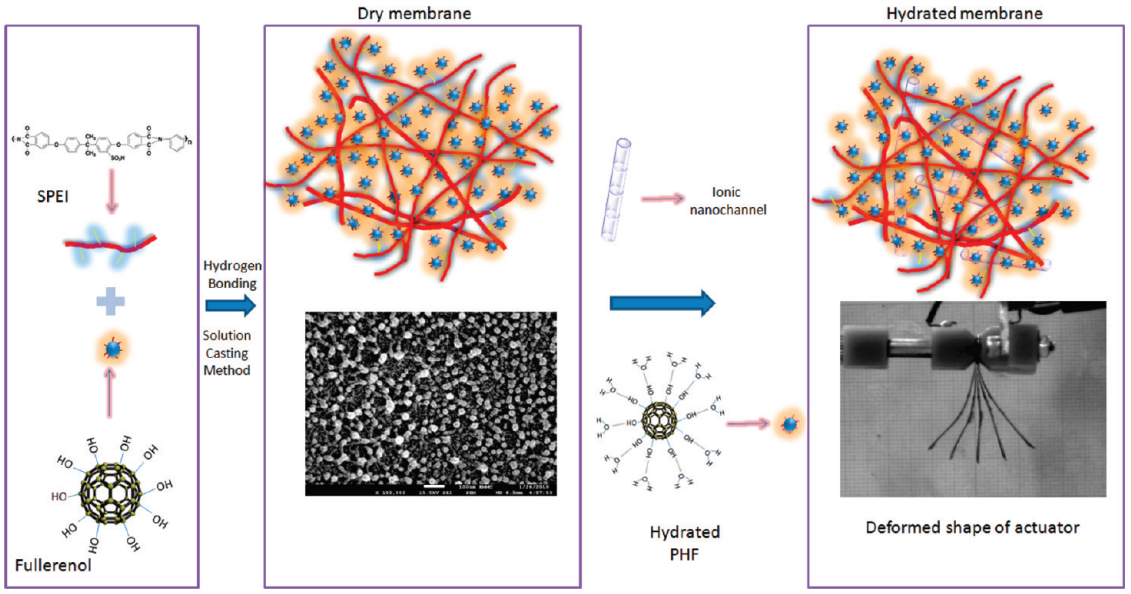

Scheme 1. Schematic illustration for fabrication of PHF and SPEI nanocomposite.

water uptake measurement at room temperature, and their ionic exchange capacity (IEC) was determined by a conventional titration method.[47,48] The proton conductivity of the well-hydrated membranes (1.76 cm^2 circle) was measured by an AC impedance analyzer (IM6e, Zahner Electrick).[49,50] The cross-sectional morphology of the pristine and platinum-coated membranes was analyzed by FE-SEM (Hitachi, S-4700). The homogeneity and surface smoothness of the nanocomposite membranes were observed by AFM (Digital Instruments, nanoscope III model).

In order to prepare actuators for actuator performance, platinum was deposited on both sides of the membranes by an electroless plating process,[51−54] after the surface of the membranes had been roughened by sand blasting. The carbon nanoparticles such as graphene, single- and multiwalled carbon nanotubes, and carbon nanofibers are widely used in electrochemical[55,56] and electromechanical actuators.[57] The electromechanical bending and hysteresis responses of the actuators were measured in deionized water by using a laser displacement sensor (LK031, Keyence) and a National Instruments data acquisition system (PXI 6252). The LabVIEW program was used with an industrial computer to acquire and control the data. The blocking force was measured by using a load cell (LVS-5GA, KYOWA) at DC 2 V in an open air atmosphere. To measure the blocking force, the tip of the actuators was directly connected to the microload cell, and the DC excitation voltage of 2 V was applied.

Acknowledgment. This work was supported by Midcareer Researcher Program through NRF grants funded by the MEST (Nos. 2010-0000300 and 2010-0018423).

REFERENCES AND NOTES

1. Kroto, H. W.; Heath, J. R.; O'brien, S. C.; Curl, R. F.; Smalley, R. E. C_{60}: Buckminsterfullerene. *Nature* **1985,** *318*, 162–163.
2. Levi, N.; Hantgan, R. R.; Lively, M. O.; Carroll, D. L.; Prasad, G. L. C60-Fullerenes: Detection of Intracellular Photoluminescence and Lack of Cytotoxic Effects. *J. Nanobiotechnol.* **2006,** *4*, 14–25.
3. Liu, J. H.; Cao, L.; Luo, P. G.; Yang, S. T.; Lu, F.; Wang, H.; Meziani, M. J.; Haque, A.; Liu, Y.; Lacher, S.; *et al.* Fullerene-Conjugated Doxorubicin in Cells. *ACS Appl. Mater. Interfaces* **2010,** *2*, 1384–1389.
4. Lebedev, B. V.; Markin, A. V.; Davydov, V. A.; Kashevarova, L. S.; Rakhmanina, A. V. Thermodynamics of Crystalline Dimer of Fullerene C60 in the Range from $T \rightarrow 0$ to 340 K at Standard Pressure. *Thermochim. Acta* **2003,** *399*, 99–108.
5. Margadonna, S.; Prassides, K. Recent Advances in Fullerene Superconductivity. *J. Solid State Chem.* **2002,** *168*, 639–652.
6. Hinokuma, K.; Ata, M. Proton Conduction in Polyhydroxy Hydrogensulfated Fullerenes. *J. Electrochem. Soc.* **2002,** *150*, A112–A116.
7. Kramer, C. N. Fullerene Research Advances. In *Photodynamic Therapy with Fullerene*; Hamblin, M. R., Mroz, P., Tegos, G. P., Gali, H., Wharton, T., Sarna, T., Pawlak, A., Eds.; Nova Science Publishers: New York, 2007; pp 1−2.
8. Gao, Y.; Grey, J. K. Resonance Chemical Imaging of Polythiophene/Fullerene Photovoltaic Thin Films: Mapping Morphology-Dependent Aggregated and Unaggregated C═C Species. *J. Am. Chem. Soc.* **2009,** *131*, 9654–9662.
9. Zakharian, T. Y.; Seryshev, A.; Sitharaman, B.; Gilbert, B. E.; Knight, V.; Wilson, L. J. A. Fullerene−Paclitaxel Chemotherapeutic: Synthesis, Characterization, and Study of Biological Activity in Tissue Culture. *J. Am. Chem. Soc.* **2005,** *127*, 12508–12509.
10. Wang, Q.; Zhang, Y.; Miyazawa, K.; Kato, R.; Hotta, K.; Wakahara, T. Improved Fullerene Nanofiber Electrodes Used in Direct Methanol Fuel Cells. *J. Phys. Conf. Ser.* **2009,** *159*, 012023.
11. Tasaki, K.; DeSousa, R.; Wang, H.; Gasa, J.; Venkatesan, A.; Pugazhendhi, P.; Loutfy, R. O. Fullerene Composite Proton Conducting Membranes for Polymer Electrolyte Fuel Cells Operating under Low Humidity Conditions. *J. Membr. Sci.* **2006,** *281*, 570–580.
12. Wang, H.; DeSousa, R.; Gasa, J.; Tasaki, K.; Stucky, G.; Jousselme, B.; Wudl, F. Fabrication of New Fullerene Composite Membranes and Their Application in Proton Exchange Membrane Fuel Cells. *J. Membr. Sci.* **2007,** *289*, 277–283.
13. Higuchi, A.; Agatsuma, T.; Uemiya, S.; Kokima, T.; Mizoguchi, K.; Pinnau, I.; Nagai, K.; Freeman, B. D. Preparation and Gas Permeation of Immobilized Fullerene Membranes. *J. Appl. Polym. Sci.* **2000,** *77*, 529–537.
14. Sterescu, D. M.; Bolhuis-Versteeg, L.; van der Vegt, N. F. A.; Stamatialis, D. F.; Wessling, M. Novel Gas Separation Membranes Containing Covalently Bonded Fullerenes. *Macromol. Rapid Commun.* **2004,** *25*, 1674–1678.
15. Hinokuma, K.; Ata, M. Fullerene Proton Conductors. *Chem. Phys. Lett.* **2001,** *341*, 442–446.
16. Li, Y. M.; Hinokuma, K. Proton Conductivity of Phosphoric Acid Derivative of Fullerene. *Solid State Ionics* **2002,** *150*, 309–315.

17. Maruyama, R. Electrochemical Mass-Flow Control of Hydrogen Using a Fullerene Based Proton Conductor. *Electrochim. Acta* **2002,** *48*, 85–89.
18. Giacalone, F.; Martin, N. Fullerene Polymers: Synthesis and Properties. *Chem. Rev.* **2006,** *106*, 5136–5190.
19. Wang, C.; Guo, Z.-X.; Fu, S.; Wu, W.; Zhu, D. Polymers Containing Fullerene or Carbon Nanotube Structures. *Prog. Polym. Sci.* **2004,** *29*, 1079–1141.
20. Jung, J. H.; Vadahanambi, S.; Oh, I.-K. Electro-Active Nano-Composite Actuator Based on Fullerene-Reinforced Nafion. *Compos. Sci. Technol.* **2010,** *70*, 584–592.
21. Chaudhuri, P.; Paraskar, A.; Soni, S.; Mashelkar, R. A.; Sengupta, S. Fullerenol-Cytotoxic Conjugates for Cancer Chemotherapy. *ACS Nano* **2009,** *3*, 2505–2514.
22. Jiao, F.; Liu, Y.; Qu, Y.; Li, W.; Zhou, G.; Ge, C.; Li, Y.; Sun, B.; Chen, C. Studies on Anti-Tumor and Antimetastatic Activities of Fullerenol in a Mouse Breast Cancer Model. *Carbon* **2010,** *48*, 2231–2243.
23. Injac, R.; Perse, M.; Obermajer, N.; Djordjevic-Milic, V.; Prijatelj, M.; Djordjevic, A.; Cerar, A.; Strukelj, B. Potential Hepatoprotective Effects of Fullerenol $C_{60}(OH)_{24}$ in Doxorubicin-Induced Hepatotoxicity in Rats with Mammary Carcinomas. *Biomaterials* **2008,** *29*, 3451–3460.
24. Chiang, L. Y.; Wang, L. Y.; Kuo, C.-S. Polyhydroxylated C_{60} Cross-Linked Polyurethanes. *Macromolecules* **1995,** *28*, 7574–7576.
25. Ouyang, J.; Zhou, S.; Wang, F.; Goh, S. H. Structures and Properties of Supramolecular Assembled Fullerenol/Poly(dimethylsiloxane) Nanocomposites. *J. Phys. Chem. B* **2004,** *108*, 5937–5943.
26. Jensen, A. W.; Wilson, S. R.; Schuster, D. I. Biological Applications of Fullerenes. *Bioorg. Med. Chem.* **1996,** *4*, 767–779.
27. Markovic, Z.; Trajkovic, V. Biomedical Potential of the Reactive Oxygen Species Generation and Quenching by Fullerenes (C60). *Biomaterials* **2008,** *29*, 3561–3573.
28. Rajagopalan, M.; Jeon, J.-H.; Oh, I.-K. Electric-Stimuli-Responsive Bending Actuator Based on Sulfonated Polyetherimide. *Sens. Actuators, B* **2010,** *151*, 198–204.
29. Shen, L.; Xu, Z.; Yang, Q.; Sun, H.; Wang, S.; Xu, Y. Preparation and Characterization of Sulfonated Polyetherimide/Polyetherimide Blend Membranes. *J. Appl. Polym. Sci.* **2004,** *92*, 1709–1715.
30. Richard, B. W.; Cheng, S. Y.; Doneva, T. A.; Oatley, D. L. Manufacture and Characterisation of Polyetherimide/Sulfonated Poly(ether ether ketone) Blend Membranes. *J. Membr. Sci.* **2005,** *250*, 1–10.
31. Tao, C. T.; Young, T. H. Polyetherimide Membrane Formation by the Cononsolvent System and Its Biocompatibility of MG63 Cell Line. *J. Membr. Sci.* **2006,** *269*, 66–74.
32. Seifert, B.; Mihanetzis, G.; Groth, T.; Albrecht, W.; Richau, K.; Missirlis, Y.; Paul, D.; von Sengbusch, G. Polyetherimide: A New Membrane-Forming Polymer for Biomedical Applications. *Artif. Organs* **2002,** *26*, 189–199.
33. Peluso, G.; Petillo, O.; Ambrosio, L.; Nicolais, L. Polyetherimide as Biomaterial: Preliminary *In Vitro* and *In Vivo* Biocompatibility Testing. *J. Mater. Sci. Mater. Med.* **1994,** *5*, 738–742.
34. Merolli, A.; Perrone, V.; Leali, P. T.; Ambrosio, L.; De Santis, R.; Nicolais, L.; Gabbi, C. Response to Polyetherimide Based Composite Materials Implanted in Muscle and in Bone. *J. Mater. Sci. Mater. Med.* **1999,** *10*, 265–268.
35. Choi, J. M.; Patel, R.; Han, J. Y.; Min, B. R. Proton Conducting Composite Membranes Comprising Sulfonated Poly(1,4-phenylene sulfide) and Zeolite for Fuel Cell. *Ionics* **2010,** *16*, 403–408.
36. Kong, L.; Tedrow, O.; Chan, Y. F.; Zepp, R. G. Light-Initiated Transformations of Fullerenol in Aqueous Media. *Environ. Sci. Technol.* **2009,** *43*, 9155–9160.
37. Kokubo, K.; Matsubayashi, K.; Tategaki, H.; Takada, H.; Oshima, T. Facile Synthesis of Highly Water-Soluble Fullerenes More Than Half-Covered by Hydroxyl Groups. *ACS Nano* **2008,** *2*, 327–333.
38. Xing, G.; Zhang, J.; Zhao, Y.; Tang, J.; Zhang, B.; Gao, X.; Yuan, H.; Qu, L.; Cao, W.; Chai, Z.; *et al.* Influences of Structural Properties on Stability of Fullerenols. *J. Phys. Chem. B* **2004,** *108*, 11473–11479.
39. Wei, W.; Zhang, C.; Du, Z.; Liu, Y.; Li, C.; Li, H. Assembly of Fullerenol Particles on Carbon Nanotubes through Poly(acryloyl chloride). *Mater. Lett.* **2008,** *62*, 4167–4169.
40. Kaushal, A. M.; Chakraborti, A. K.; Bansal, A. K. FTIR Studies on Differential Intermolecular Association in Crystalline and Amorphous States of Structurally Related Non-Steroidal Anti-Inflammatory Drugs. *Mol. Pharmaceutics* **2008,** *5*, 937–945.
41. Guo, Z.-X.; Sun, N.; Li, J.; Dai, L.; Zhu, D. Nanoscale Aggregation of Fullerene in Nafion Membrane. *Langmuir* **2002,** *18*, 9017–9021.
42. Sudeep, P. K.; Ipe, B. I.; Thomas, K. G.; George, M. V.; Barazzouk, S.; Hotchandani, S.; Kamat, P. V. Fullerene-Functionalized Gold Nanoparticles. A Self-Assembled Photoactive Antenna-Metal Nanocore Assembly. *Nano Lett.* **2002,** *2*, 29–35.
43. Markovic, B. T.; Jovanovic, S.; Jokanovic, V.; Nedic, Z.; Dramicanin, M.; Markovic, Z. Atomic Force Microscopy Study of Fullerene-Based Colloids. *Appl. Surf. Sci.* **2008,** *255*, 3283–3288.
44. Lee, C. H.; Lin, T. S.; Lin, H. P.; Zhao, Q.; Liu, S. B.; Mou, C.-Y. High Loading of C60 in Nanochannels of Mesoporous MCM-41 Materials. *Microporous Mesoporous* **2003,** *57*, 199–209.
45. Ding, J.; Chuy, C.; Holdcroft, S. A Self-Organized Network of Nanochannels Enhances Ion Conductivity through Polymer Films. *Chem. Mater.* **2001,** *13*, 2231–2233.
46. Klaus, S.-R.; Chen, Q. Parallel Cylindrical Water Nanochannels in Nafion Fuel-Cell Membranes. *Nat. Mater.* **2008,** *7*, 75–83.
47. Kerres, J.; Cui, W.; Disson, R.; Neubrand, W. Development and Characterization of Crosslinked Ionomer Membranes Based upon Sulfinated and Sulfonated PSU Crosslinked PSU Blend Membranes by Disproportionation of Sulfinic Acid Groups. *J. Membr. Sci.* **1998,** *139*, 211–225.
48. Kim, D. S.; Guiver, M. D.; Nam, S. Y.; Yun, T. I.; Seo, M. Y.; Kim, S. J.; Hwang, H. S.; Rhim, J. W. Preparation of Ion Exchange Membranes for Fuel Cell Based on Crosslinked Poly(vinyl alcohol) with Poly(styrene sulfonic acid-*co*-maleic acid). *J. Membr. Sci.* **2006,** *281*, 156–162.
49. Barique, M. A.; Wu, L.; Takimoto, N.; Kidena, K.; Ohira, A. Effect of Water on the Changes in Morphology and Proton Conductivity for the Highly Crystalline Hydrocarbon Polymer Electrolyte Membrane for Fuel Cells. *J. Phys. Chem. B* **2009,** *113*, 15921–15927.
50. Lu, J.; Kim, S. G.; Lee, S.; Oh, I.-K. A Bio-Mimetic Actuator Based on an Ionic Networking Membrane of Poly(styrene-*alt*-maleimide)-Incorporated Poly(vinylidene fluoride). *Adv. Funct. Mater.* **2008,** *18*, 1290–1298.
51. Jeon, J.-H.; Cheng, T.-H.; Oh, I.-K. Snap-Through Dynamics of Buckled Actuator. *Sens. Actuators, A* **2010,** *158*, 300–305.
52. Jeon, J.-H.; Oh, I.-K. Selective Growth of Platinum Electrodes for MDOF Actuators. *Thin Solid Films* **2009,** *517*, 5288–5292.
53. Wang, X.-L.; Oh, I.-K.; Cheng, T.-H. Electro-Active Polymer Actuators Employing Sulfonated Poly(styrene-*ran*-ethylene) as Ionic Membranes. *Polym. Int.* **2010,** *59*, 305–312.
54. Wang, X.-L.; Oh, I.-K.; Lee, S. Electro-Active Artificial Muscle Based on Cross-Linked PVA/SPTES. *Sens. Actuators, B* **2010,** *150*, 57–64.
55. Juluri, B. K.; Kumar, A. S.; Liu, Y.; Ye, T.; Yang, Y.-W.; Flood, A. H.; Fang, L.; Stoddart, J. F.; Weiss, P. S.; Huang, T. J. A Mechanical Actuator Driven Electrochemically by Artificial Molecular Muscles. *ACS Nano* **2009,** *3*, 291–300.
56. Xie, X.; Qu, L.; Zhou, C.; Li, Y.; Zhu, J.; Bai, H.; Shi, G.; Dai, L. An Asymmetrically Surface-Modified Graphene Film Electrochemical Actuator. *ACS Nano* **2010,** *4*, 6050–6054.
57. Wang, X.-L.; Oh, I.-K.; Kim, J.-B. Enhanced Electromechanical Performance of Carbon Nano-Fiber Reinforced Sulfonated Poly(styrene-*b*-[ethylene/butylene]-*b*-styrene) Actuator. *Compos. Sci. Technol.* **2009,** *69*, 2098–2101.